Pure & Appl. Chem., Vol. 63, No. 12, pp. 1733–1742, 1991.
Printed in Great Britain.

Molecular dynamics studies of platinum/water interfaces

K. Heinzinger

Max-Planck-Institut für Chemie (Otto-Hahn-Institut), D-6500 Mainz, Germany

Abstract - The results of Molecular Dynamics simulations of a water lamella between platinum crystals and of water on a Pt(100) surface for different degrees of coverage with and without homogeneous electrical field are reported. In addition, first results of the effect of the surface on the hydration of ions are presented. The flexible BJH model of water is employed and the Pt-water and Pt-ion interaction potentials are derived from molecular orbital calculations. It is demonstrated that the influence of the Pt(100) surface on the structural and dynamical properties of water is significant only for the adsorbate layer but depends on the degree of coverage.

INTRODUCTION

The first paper on computer simulations of water/metal interfaces was published only a few years ago (ref. 1) while simulations of water near other kinds of solid walls were reported as early as 1981. They have been reviewed recently (ref. 2) and will, therefore, not be discussed here.

In the MD simulation reported by Spohr and Heinzinger (ref. 1) as well as in the MC studies by Parsonage and Nicholson (ref. 3) and by Gardner and Valeau (ref. 4) the metallic character of the uncharged wall was described by image forces. In all cases a strong preference for an orientation of the dipole moment of the water molecules parallel to the surface resulted from the simulations, but an average angle of 90° between the vector normal to the surface and the dipole moment does not agree with the work function change measured for water adsorption on Pt(100)(ref. 5), Ni(100)(ref. 6), Ni(111)(ref. 7), and Ag(110)(ref. 8). In the case of the corrugated surface (ref. 1) the water-wall potential used has led to a preferential adsorption on the hollow sites of the surface, which is also in contradiction to several quantum mechanical calculations. They indicate that an adsorption on top of the metal atom is the preferred site (ref. 9-11).

Therefore, it seemed to be appropriate to try to find a water-metal potential which leads to better agreement between simulation on one side and experiments and MO calculations on the other. Consequently the potential used by Spohr (ref. 12) is based on extended Hückel molecular orbital calculations of a platinum cluster with a water molecule (ref. 13). A further improvement is achieved by employing a flexible model for the description of the water-water interactions (ref. 14). Foster et al. (ref. 15) confirmed these results in a more recent MD study employing a similar potential for the Pt-water interactions and extended the investigations to the simulation of water near a Pt(111) surface (ref. 16).

The results achieved with the potentials proposed by Spohr concern not only structural (ref. 12) and dynamical (ref. 17) properties of a water lamina but have been extended also to simulations with partial coverages of the Pt-surface (ref. 18) and with charged surfaces (ref. 19,20). As these investigations are the by far most extensive ones, this review will mainly concentrate on them. Finally, based on the Pt-ion potentials proposed by Seitz-Beywl et al. (ref. 21) first results of the effect of the Pt(100) surface on the hydration of ions are discussed (ref. 22).

INTERACTION POTENTIALS

The water-water interactions employed in the simulations are described by the flexible BJH model (ref. 14) which has proved its usefulnes in various simulations of pure water and aqueous electrolyte solutions (see e.g. ref. 23). The platinum-platinum interactions are modeled by a harmonic nearest-neighbor potential (ref. 24) in order to account for the coupling between motions of the water molecules and lattice vibrations.

The analytical form of the platinum-water potential has been proposed by Spohr (ref. 12). It is based on the extended Hückel molecular orbital calculations by Holloway and Bennemann of a water molecule on top of a five-atom platinum cluster (ref. 13). This potential leads to the preferential adsorption site on top of a platinum atom. The energetically most favorable orientation is the one where the dipole moment vector points away from the surface in agreement with the Hückel calculations, with a minimum of the total interaction energy between one water molecule and all Pt atoms of 35.7 kJ/mol. In Fig. 1b the total potential energy is given as a function of the x- and y-coordinates for a water-Pt(100) surface distance Δz chosen such that the potential has its minimum. The figure shows again clearly that the potential leads to a surface corrugation with deep energy minima at the platinum atom positions.

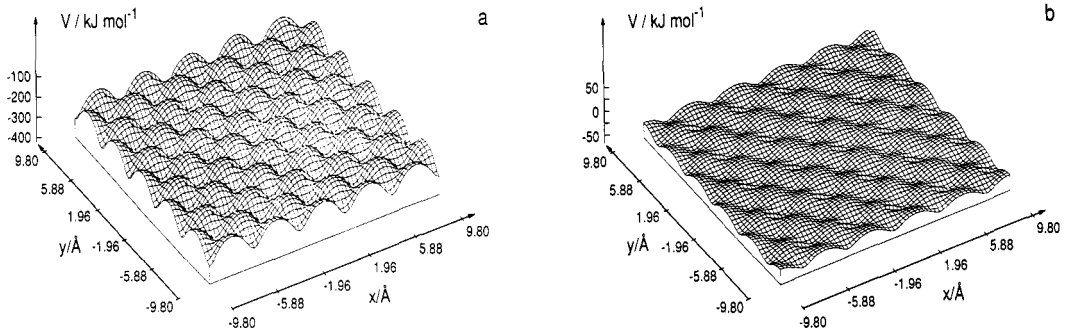

Fig. 1. Water-metal (b) and I^--metal (a) interaction potentials as a function of x and y for a distance Δz chosen in such a way that the potential has its minimum value. The dipole moment vector of the water molecule points away from the surface (ref. 12,21).

The platinum-I^- and platinum-Li^+ potentials are derived from molecular orbital calculations of one ion and a platinum cluster consisting of nine and five atoms, respectively (ref. 21). The total potential energy of one I^- in the field of an infinitly extended platinum crystal as a function of the x- and y-coordinates is presented in Fig. 1a as example. The distance between the ion and the Pt(100) surface Δz is chosen again such that the potential has its minimum. The surface corrugation is by about a factor of 10 more pronounced than in the platinum-water case. Both ions are absorbed preferentially opposite of a hollow site of the Pt(100) surface and the lowest potential minima for Li^+ and I^- are found at -265 and -319 kJ/mol, respectively.

For further details of the potentials the reader is referred to the original publications cited.

DETAILS OF THE SIMULATIONS

This review will concentrate on the presentation of results from five different simulations. Two investigations are concerned with a water lamina - with (ref. 19,20) and without (ref. 12,17) an applied electrical field. In both cases the rectangular basic box has side lengths $L_x = L_y = 19.6$Å and $L_z = 45$ Å and is shown in Fig. 2b. The interval $-12.7 < z < 12.7$ Å is occupied by 305 water molecules, and in the regions $12.7 \leq |z| \leq 22.5$ Å 550 platinum atoms are located. As a consequence of the introduction of periodic boundary conditions in all directions, the platinum subsystem can be regarded as one infinitely extended slab with a thickness of 19.6 Å which interacts with water molecules on both surfaces. The values of L_x and L_y have been chosen in accordance with the periodicity of the face-centered-cubic platinum lattice with a lattice constant $\alpha = 3.92$Å. The crystal slab consists of 5 x 5 x 5 face-centered-cubic unit cells, each containing four atoms and the (100) plane being parallel to the (xy) plane of the periodic box. In Fig. 2a the surface geometry is sketched by circles and crosses denoting surface atoms and second layer atoms, respectively.

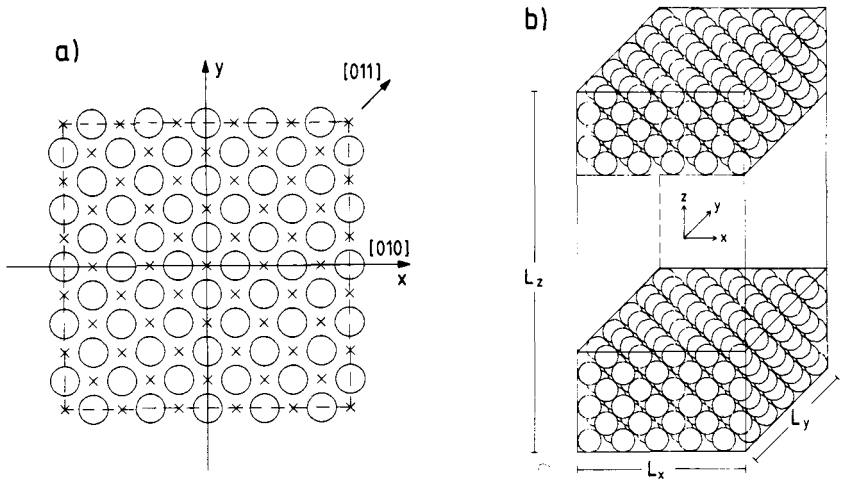

Fig. 2. (a) Sketch of the arrangement of surface platinum atoms (circles) and second-layer platinum atoms (crosses) in the (xy) plane of the basic cell. The dashed lines are the periodic boundaries of the basic cell at $x,y = \pm 9.8$ Å. The [010] and [011] directions of the crystal are indicated. (b) Sketch of the basic tetragonal simulation cell. The water molecules are located in the center of the box, and the platinum atoms are represented by the circles. The coordinate system which is used throughout the paper is sketched in the center (ref. 12).

Two more kinds of simulations deal with the properties of water again on a Pt(100) plane but with only a limited degree of coverage θ where θ is defined as the number ratio of water molecules and platinum atoms at the surface. The basic box is the same as in the other simulations but with a smaller number of water molecules according to the chosen value for θ. Simulations were performed for θ values of 0.2, 0.4, 0.6, 0.8 and 1.4 without and for $\theta = 1$ with applied electrical fields (refs. 18-20).

Finally, first results are reported from a simulation of an aqueous LiI solution again in contact with a Pt(100) surface. The basic box is in the x- and y-directions the same as in the case of the lamina but the surface is covered by only three layers of water molecules and one Li^+ or one I^- is positioned in the contact layer. The ions do not leave this layer during the whole simulation time of 7.5 ps (ref. 22).

RESULTS AND DISCUSSION

Density profiles

The first properties to be calculated as far as the structure of a water/metal interface is concerned are the oxygen and hydrogen atom density profiles. They are shown in Fig. 3a. The first maxima of both profiles coincide at a distance of about 2.5 Å from the Pt surface and the reduced oxygen atom density is by about 30% higher than that of the hydrogen atoms. After a much less pronounced second peak in both density profiles the distributions become uniform except for statistical noise.

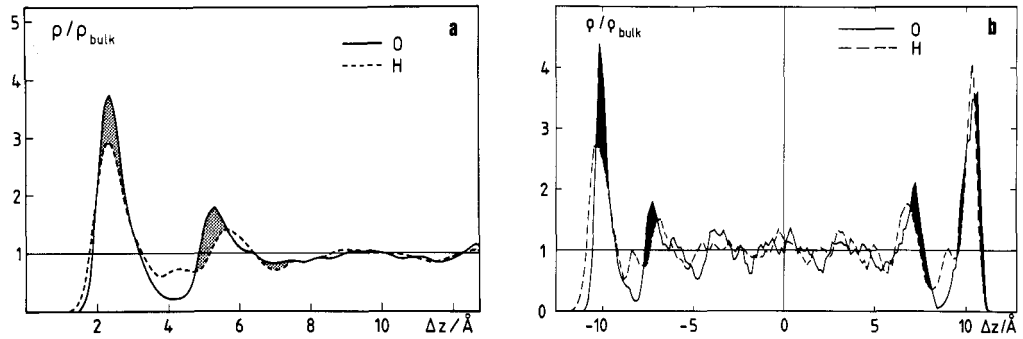

Fig. 3. Normalized oxygen and hydrogen atom densities as a function of distance from the two Pt(100) surfaces without electrical field (a) and after application of a homogeneous electrical field of 10^{10} V/m (b). The shaded areas indicate an excess of negative charges (ref. 19).

The coincidence of the positions of the first peaks indicates a strong preference for a water molecule orientation parallel to the Pt surface. As the potential minimum for a single water molecule is found for an orientation where the dipole moment vector points away from the surface, this coincidence demonstrates that the water-water interactions predominantly determine the structure of even the first water layer.

The immediate consequence of the application of a homogeneous electrical field is a change in the orientation of the water molecules between the Pt-walls. This reorientation leads not only to an assymmetry in the height of the density profiles with respect to the two walls but also to slight changes in the position of the maxima of ρ_O and ρ_H as can be seen from Fig. 3b where the density profiles are shown for the same system as discussed in the preceding paragraph (Fig. 3a) but with an applied field of 10^{10}V/m. The resulting differences in the charge density can be seen from Fig. 3b where again the excess of negative charges are marked by shaded areas. (A quantitative comparison of the profiles in Fig. 3 is not possible because the temperatures for which the two simulations have been performed differ by about 50° C). The potential profiles resulting from the differences in charge density will be discussed below.

Pair correlation functions

The strong water-surface interaction together with the corrugation of the surface gives rise to much more drastic changes in water structure than the ones observed in previous computer simulations of water near smooth unpolar surfaces (see references in ref. 2). The arrangement of the adsorption sites in a quadratic grid with a spacing of 2.77 Å allows on the one hand the formation of hydrogen bonds between pairs of adsorbed molecules but is on the other hand not compatible with the tendency to form a local tetrahedral network like in bulk water. Hence, considerable changes of the atom-atom pair correlation functions (PCFs) are expected close to the surface. All PCFs have been calculated according to the defining relation

$$g(\vec{r}_1, \vec{r}_2) = \frac{\rho^{(2)}(\vec{r}_1, \vec{r}_2)}{\rho^{(1)}(\vec{r}_1) \cdot \rho^{(1)}(\vec{r}_2)} \tag{1}$$

with $\rho^{(i)}$ the local i-particle density and $\vec{r}_1$ and $\vec{r}_2$ the Cartesian coordinates of the two particles.

In order to get a closer view on the correlations between adsorbed molecules ($\Delta z \leq 4.2$ Å), the PCFs $g_{OO}(x,y)$, $g_{LiO}(x,y)$ and $g_{IO}(x,y)$ are plotted in Fig. 4(a). x and y are the components of the interparticle vector along the two laboratory frame axes parallel to the surface (Fig. 2a). The origin of the coordinate system coincides for $g_{OO}(x,y)$ with the position of a Pt atom and for $g_{LiO}(x,y)$ and $g_{IO}(x,y)$ practically with a hollow site.

The far-ranging symmetrical arrangement of high maxima in the oxygen-oxygen PCF indicates the formation of a quadratic overlayer commensurate with the crystal periodicity. The O–O correlation is obviously not due to water-water interactions but a consequence of the quadratic arrangement of adsorption sites.

The effect of the surface on the ion-oxygen PCFs depends strongly on the size of the ion. In the case of Li^+ where the first maximum in $g_{LiO}(r)$ appears at 2 Å the ion fits nicely into a hollow site of the quadratic water overlayer and consequently the PCF is significantly more pronounced than in the bulk. It is reverse for the I-O PCF with the first peak positioned at 3.5 Å. The I^- moves in an area between a hollow and a bridge site. Therefore, oxygen atoms can be found only on top of two of the four neighbouring Pt atoms which means a significant broadening of the peaks in $g_{IO}(r)$ (ref. 22).

Orientation of the water molecules

The orientation of the 305 water molecules in the lamina will be described in this section by the normalized distributions of the cosine of the angle between the outward directed surface normal and the dipole vector, ϑ_μ. In order to get information about the dependence of the orientation on the distance from the surface the lamina is subdivided into 6 slabs of 4.2 Å each. The first two slabs near the walls extend over the range of the first peak in the oxygen atom density profile (Fig. 3). The next two slabs correspond to the second peak while the remaining two inner slabs have bulk water density. The results are presented in Fig. 4b.

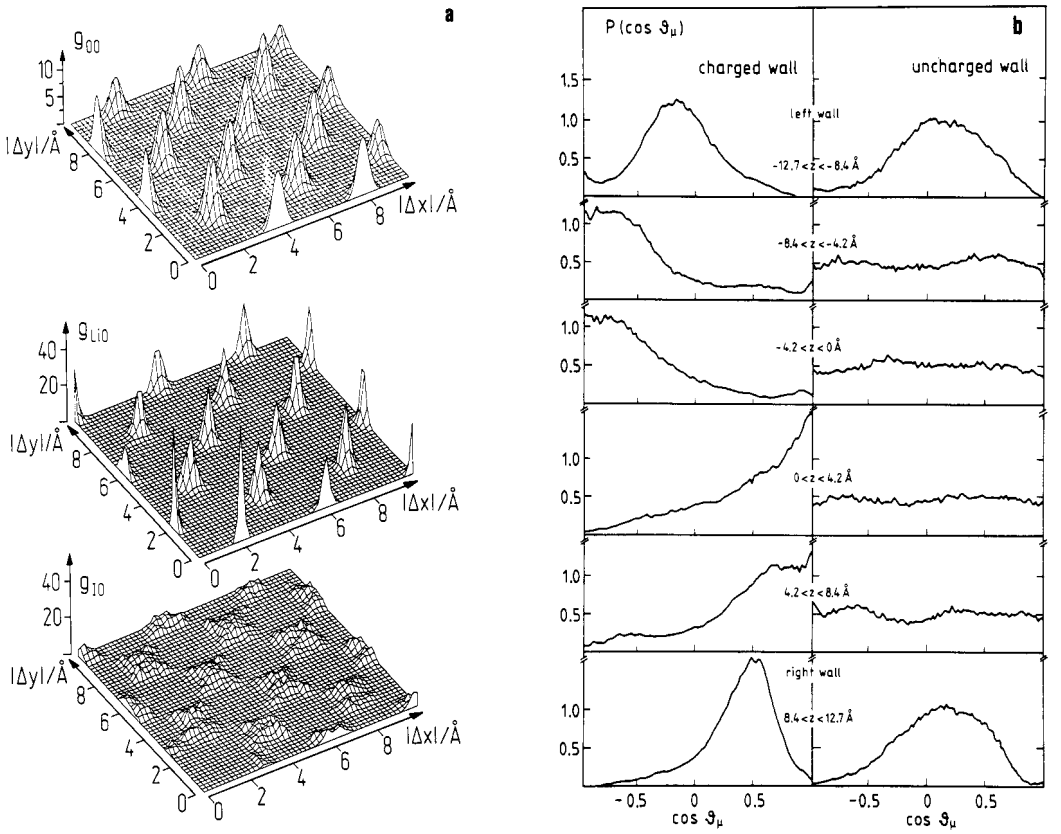

Fig. 4(a). Oxygen-oxygen, lithium-oxygen and iodide-oxygen pair correlation functions in the adsorbed layer ($\Delta z \leq 4.2$ Å for all particles). x and y are the projections of the interatomic distance on the x and y directions of the laboratory coordinate system (refs. 12,22).

Fig. 4(b). Distributions of the cosine of the angle ϑ_μ between the dipole unit vector $\hat{\mu}$ and the outward directed surface normal $\hat{z}$ in 6 distance intervals from the surface calculated from a simulation with an electrical field of 10^{10} V/m (left) and without an electrical field (right) (ref. 19).

In the field free case pronounced deviations from a uniform distribution are found for the wall layers only indicating a preference for an angle slightly smaller than 90°. With this definition of ϑ_μ and the fact that necessarily the surface normal vectors point in opposite directions in the center of the slab the distributions are symmetric with respect to the walls in the field free case. Small differences between left and right wall indicate the statistical uncertainty. In the second slab and in the center of the lamina the distributions are uniform within the limits of statistical error.

The immedate consequence of the application of the homogeneous electrical field of 10^{10} V/m is a change in the orientation of the water molecules between the Pt-walls (left column in Fig. 4b). The distributions become asymmetric. The field causes shifts of the maxima of the distributions in different directions close to the two walls and the distributions in the inner layers, which were uniform in the field free case, show strong preferences.

Electrical potential profiles

The electrostatic potential profile can be calculated from the charge density profile as marked by the shaded areas in Fig. 3 or from the dipole moment densities $\rho_\mu(z)$ presented in Fig. 5a for both cases - calculated from the cos ϑ_μ distributions depicted in Fig. 4b - through

$$\Phi(z) = \frac{1}{\varepsilon_0} \int_{z_w}^{z} \rho_\mu(z')\mathrm{d}z' - E_0 \cdot (z - z_w) + \Phi(z_w) \qquad (2)$$

where Φ is the electric potential, ε_0 the vacuum permittivity, E_0 the external field strength and

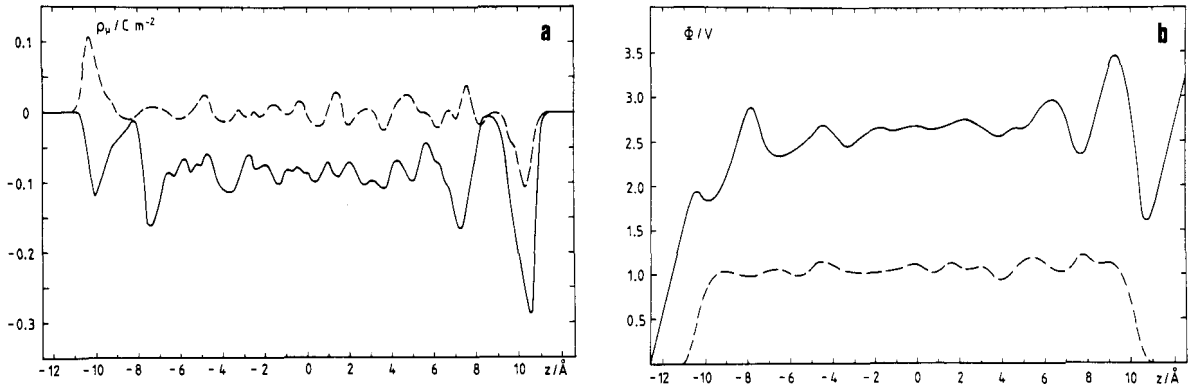

Fig. 5. Dipole density (a) and electrostatic potential (b) profiles perpendicular to the platinum walls. The solid line is calculated from a simulation with an electric field of 10^{10} V/m while the dashed line is without electric field (ref. 19).

z the coordinate perpendicular to the walls with z_w = -12.7 Å. The resulting electrical potential profiles are shown in Fig. 5b with $\Phi(z_w) = 0$ for z_w = -12.7 Å.

For the external field free system $\Phi_\mu(z)$ is symmetric in the center of the lamina - except for statistical noise. The potential drop is calculated to be 1.1 V. The applied electrical field breaks the symmetry. The potential difference $\Delta\Phi$ is 3.3 V between the two walls. There is a linear increase of $\Phi(z)$ in the particle free regions next to the walls. The potential strongly oscillates in the range of the first and even of the second water layer where the Pt-water interaction plus the applied field are effective. In the middle of the lamina $\Phi(z)$ is almost linear as expected for a homogeneous dielectric. The corresponding average electric field is E_{av} = (-1.81 ± 0.23) 10^8V/m. The dielectric constant of the bulk water can be calculated from the ratio of E_0 and E_{av} resulting in $\varepsilon_{\text{bulk}} = 55 \pm 7$. This is definitely less than the normal value of bulk water. Under the influence of high electric fields the dielectric constant lowers because of the saturation effect in a way predicted by the Kirkwood-Booth theory (ref. 25). Inserting E_{av} into Booth's equation $\varepsilon_{\text{Booth}} = 61 \pm 14$ is obtained. The agreement between these two values is satisfactory. From the potential drops in the interphases one may estimate local dielectric constants of $\varepsilon \approx 5$ in accordance with models of the solid/aqueous solution interface which assume a strongly reduced dielectric constant in the adsorbed layer (ref. 26).

In order to check the reliability of these potential profiles the potential drop at the Pt(100) surface has been calculated in the field free case for various degrees of coverage θ. These results can be compared - at least qualitatively - with experimental work function changes for the adsorption of water on Ni(100) (ref. 6), Ni(111) (ref. 7), and Ag(110) (ref. 8).

The dipole density ρ_μ as shown in Fig. 6 for various degrees of coverage is confined to a range $z \leq 3.2$ Å even at $\theta = 1.4$. This indicates that the orientations of the molecules adsorbed in the outer range of the first layer are more or less random which may be due to the fact that they are partially bound to adsorbed water molecules and partially to the crystal directly. The second layer produces a slightly negative dipole density which means that the dipole moment vector points preferentially towards the surface. For the sub-monolayer coverages ($\theta \leq 0.8$) the dipole moment density increases until $\theta = 0.6$ and remains constant for $\theta = 0.8$. At $\theta = 1.4$ the small additional contribution observed in the first layer is balanced by the negative contribution in the second layer.

In Fig. 7 the simulated values of the potential drop as a function of θ calculated from the dipole moment densities (Fig. 6) according to Eq.(2) are compared with experimental work function changes mentioned above. The simulation results reproduce the experimental trend very well. After a steep initial decrease $-\chi(\infty)$ remains constant for the coverages above about 0.5. The experimental results show a further decrease which is, however, significantly smaller than that for small θ. Quantitative agreement can be expected only from simulations which take explicitly into account the electronic structure of water and especially that of the metal (ref. 18). It should be mentioned here that preliminary results of computer simulations show

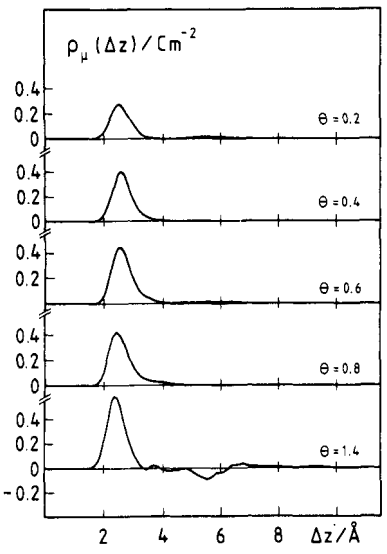

Fig. 6. Dipole density as a function of distance from the surface for various degrees of coverage θ (ref. 18).

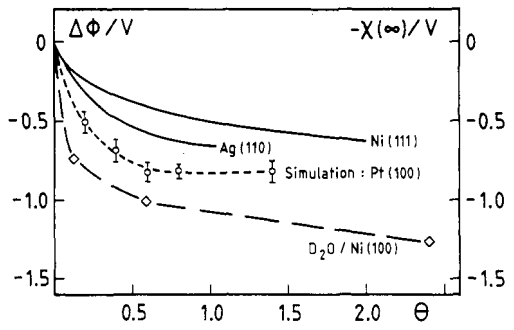

Fig. 7. Comparison of experimental and calculated values of the work function change. The data are taken from (ref. 9) for H_2O on Ni(111), from (ref. 10) for H_2O on Ag(110), and from (ref. 8) for D_2O on Ni(100) (diamonds). Dashed lines are drawn to guide the eyes while full lines are from the published curves. Error bars are not available for experimental results (ref. 18).

that the work function change depends linearily on the strength of the applied homogeneous electrical field in the range $10^9 - 10^{10}$ V/m (ref. 20).

Self-diffusion coefficients and hindered translational motions

The self-diffusion coefficients can be determined from the simulation either by the mean square displacement:

$$D = \lim_{t\to\infty} \langle [\vec{R}(t) - \vec{R}(0)]^2 \rangle / 6t \tag{3}$$

or - as done here - through the velocity autocorrelation functions with the help of the Green-Kubo relation:

$$D = \lim_{t\to\infty} \frac{1}{3} \int_0^t \langle \vec{v}(0) \cdot \vec{v}(t') \rangle dt'. \tag{4}$$

The averages have been calculated according to:

$$\langle \vec{v}(0) \cdot \vec{v}(t) \rangle = \frac{1}{N_T N} \sum_{i=1}^{N_T} \sum_{j=1}^{N} \vec{v}_j(t_i) \cdot \vec{v}_j(t_i + t) \tag{5}$$

where N denotes the number of particles, N_T the number of time averages and $\vec{v}_j(t)$ the velocity of particle j at time t.

The velocity autocorrelation functions have been calculated separately for three different layers as well as for the components parallel and perpendicular to the surface. They are shown in Fig. 8a for the simulation without an external electrical field. After the application of a field of 10^{10}V/m the velocity autocorrelation functions for the adsorbed layers ($\Delta z \leq 4.2$ Å) at the left and right wall become different: But the differences are hardly outside the limits of statistical uncertainty and are, therefore, not shown here.

The self-diffusion coefficients calculated according to Eq.(4) are given in Table 1 relative to those of pure BJH water in order to compare the results from the simulations with and without electrical field which have been performed at temperature of 305° and 349° K, respectively. It can be seen from Table 2 that for the field free case the self-diffusion coefficients parallel as well as perpendicular to the surface for the water molecules in the adsorbate layer are too small to be calculated accurately from the simulation which extended over about 9 ps. In the third layer the self-diffusion coefficients are the same for both directions and do not differ from

TABLE 1. Self-diffusion coefficients of the water molecules relative to pure water calculated separately for the motions parallel and perpendicular to the platinum surface for three different layers as well as with and without an external electrical field. Δz denotes the distance between the oxygen atoms and the surface in Å. The self-diffusion coefficients for pure BJH water at temperatures of 349° and 305° C are found to be (3.1 ± 0.2) and (2.0 ± 0.2) $10^{-5}cm^2s^{-1}$, respectively (ref. 27).

		$D_{\parallel}$		$D_{\perp}$	
Layer[Å] \ E_0[V/m]		0	10^{10}	0	10^{10}
$\Delta z \leq 4.2$	L	< 0.1	< 0.1	< 0.1	< 0.1
	R	< 0.1	< 0.1	< 0.1	≈ 0.2
$4.2 < \Delta z \leq 6.2$		1.2	0.8	0.4	0.3
$6.2 < \Delta z$		1.0	1.1	1.0	0.7

that of pure water in the limits of error. An interesting feature is found for the second layer. The self-diffusion perpendicular to the surface is strongly reduced for these water molecules as the strongly attached adsorbate layer allows a mobility only in one direction. By contrast, the self-diffusion parallel to the surface is increased as the number of hydrogen bonds between first and second layer is smaller than in pure water.

The external electrical field leads - as in several structural properties - to an anisotropy in the self-diffusion coefficients of the water molecules in the wall layers. The reduction in $D_{\parallel}$ relative to pure water remains more than 90% just as in the field free case, but the electrical field makes the motions perpendicular to the wall at the right side significantly easier without a change at the left wall. The anisotropy in the intermediate and the bulk layer is smaller than the statistical uncertainty and the relative self-diffusion coefficients in these layers remain either unchanged or decrease after an application of an external field of 10^{10}V/m. This is a consequence of the structural changes resulting from the reorientation of the water molecules in the field as discussed above.

The Fourier transformations of the center-of-mass velocity autocorrelation functions give the spectral densities of the hindered translational motions of the water molecules. They are shown in Fig. 8b. They are very similar to those of pure BJH water for the second and third layer water molecules - for both motions parallel and perpendicular to the surface (ref. 28). The first maximum at about 50 cm^{-1} is usually assigned to O-O-O flexing motions and the broad band around 200 cm^{-1} to O-O stretching motions (ref. 29). For the adsorbate layer the motions parallel and perpendicular to the surface can, therefore, be assigned mainly to O-O stretching and O-O-O bending modes, respectively. The spectrum of the perpendicular motion also includes the O-Pt stretching motion.

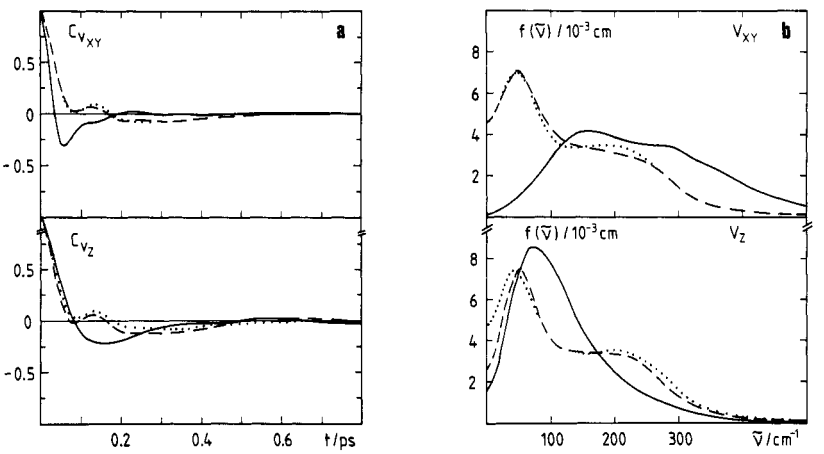

Fig. 8. Center-of-mass velocity autocorrelation functions (a) and spectral densities of the hindered translations of the water molecules (b) for the motions parallel (top) and perpendicular (bottom) to the surface for three different layers, defined by $\Delta z \leq 4.2$ Å (full), $4.2 < \Delta z \leq 6.2$ Å (dashed), and $6.2 < \Delta z$ (dotted) where Δz denotes the distance of the oxygen atom from the surface (ref. 17).

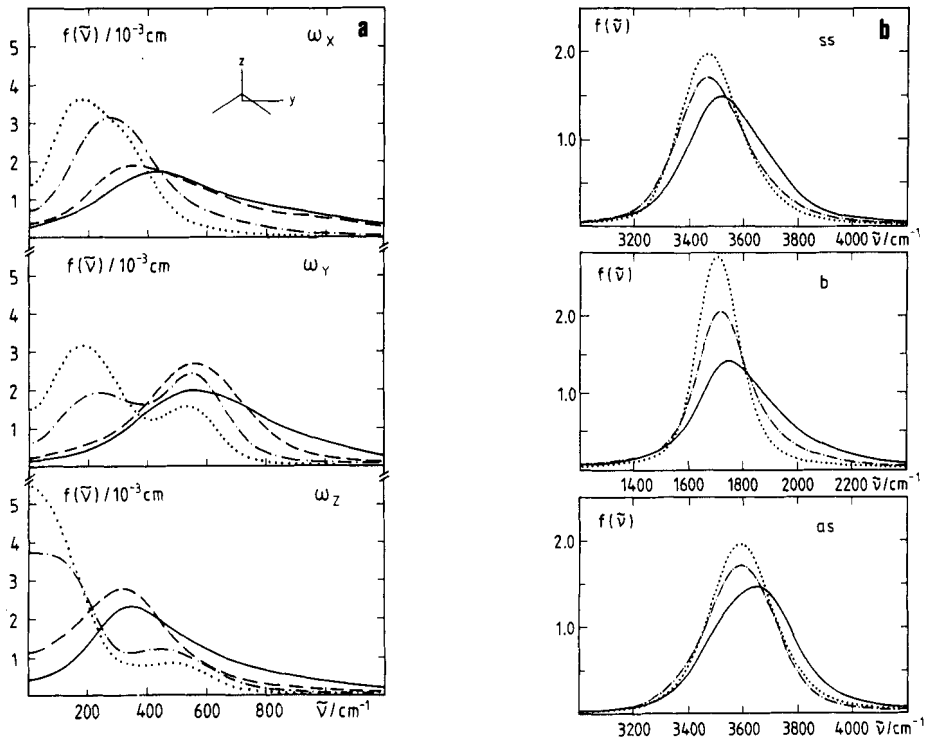

Fig. 9a. Spectral densities of the librations around the three main axes of the water molecule as defined in the insertion, calculated for different degrees of surface coverage θ. The full line gives the results for the adsorbate layer of the complete system while dashed, dash-dotted, and dotted lines are for surface coverages of 0.2, 0.4 and 0.8, respectively (ref. 31).

Fig. 9b. Spectral densities of the intramolecular vibrations (top to bottom: symmetric stretch, bend, asymmetric stretch) of the water molecules in the adsorbed layers on the left (dash-dotted) and the right (full) wall as well as in the bulk. The applied electrical field is 10^{10} V/m. The wall and bulk layers are defined by O-Pt distances $\Delta z \leq 4.2$ Å and $\Delta z > 6.2$ Å, respectively (ref. 19).

TABLE 2. Frequencies of the maxima in cm^{-1} in the spectral densities of the librational (ω), and vibrational (ν) modes of the water molecules in the wall layers and in the bulk. LW and RW indicate the left (negative) and the right (positive) wall in the case of an external electrical field of 10^{10} V/m (ref. 19) while W denotes the field free case (ref. 17). The statistical uncertainities are estimated to be about ± 10 cm^{-1}.

	ω_x	ω_y	ω_z	bend	ss	as
LW	450	590	340	1750	3520	3650
W	430	560	350	1740	3480	3620
RW	450	590	410	1720	3470	3590
B	430	590	410	1710	3480	3600

Therefore, the strong attachment of the water molecules to the surface in the adsorbate layer results in a blueshift of the 200 and the 50 cm^{-1} band for the motions parallel and perpendicular to the surface, respectively. At the same time the intensities of the supplementary bands decrease strongly. Ibach and Lehwald have investigated water on a Pt(100) surface by high resolution electron energy loss spectroscopy (ref. 30). They assigned the band at 240 cm^{-1} to the O-O stretching vibration in agreement with the results presented here. It is not clear why a second band at 460 cm^{-1}, which has been assigned by these authors to the O-Pt stretching motion, cannot be found in the spectral densities of the hindered translational motions calculated from the simulation. It has been mentioned above that the difference between the autocorrelation functions calculated from the simulations with and without an external electrical field are rather small. Accordingly, the same is true for the spectral densities of the hindered translational motions. They are, therefore, not shown here. For details the reader is referred to ref. 19.

Librational motions and intramolecular vibrations

The scheme used to separate the various librational and vibrational modes of the water molecules has been described in ref. 32. The effect of the surface as well as that of the external field on the librational motions of the water molecules seems to be quite small. This can be seen from Table 2 where the positions of the peak maxima are presented. For a discussion of the few significant differences the reader is referred to refs. 17 and 19.

The effect of the water-water interaction on the spectral densities of the librations around the three main axes are shown in Fig. 9a for different degrees of coverage. With decreasing coverage the maxima either shift to or a second maximum appears at lower frequencies for all three librations. The rotation around the z-axis becomes almost free for coverages of 0.2 and 0.4. Even for $\theta = 0.2$ the intensity in the range of the pure water band does not become zero. This is a consequence of the result that at low coverage the water molecules are not uniformly distributed over the surface but form clusters.

It can be seen from Table 2 and Fig. 9b that the external electrical field of 10^{10} V/m causes an anisotropy in the spectral densities of all three intramolecular vibrations. The frequency maxima at the right wall appear, within the limits of statistical uncertaintity, at the same position as those for the bulk water. But in all cases there is a blueshift at the left (negatively charged) wall. A possible explanation, at least as far as the O-H stretching vibrations are concerned, is based on structural considerations. At the left wall the hydrogen atoms of the water are nearer to the surface than the oxygen (Fig. 3). This in turn could mean smaller chances for hydrogen bonding and consequently higher frequencies than at the right wall where the OH bonds point more towards the bulk (Fig. 4b). A weaker hydrogen bonding would also explain the broadening of the peaks near the left wall.

Acknowledgement Financial support by Deutsche Forschungsgemeinschaft is gratefully acknowledged.

REFERENCES

1. E. Spohr and K. Heinzinger, *Chem. Phys. Lett.*, *123*, 218 (1986).
2. E. Spohr and K. Heinzinger, *Electrochim. Acta*, *33*, 1211 (1988).
3. N.G. Parsonage and D. Nicholson, *J. Chem. Soc. Faraday Trans. II*, *82*, 1521 (1986); *83*, 663 (1987).
4. A.A. Gardner and J.P. Valleau, *J. Chem. Phys.*, *86*, 4171 (1987).
5. E. Langenbach, A. Spitzer and H. Lüth, *Surf. Sci.*, *147*, 179 (1984).
6. D.E. Peebles and J. M. White, *Surf. Sci.*, *144*, 512 (1984).
7. C. Nöbl and C. Benndorf, *Surf. Sci.*, *182*, 499 (1987).
8. K. Bange, T.E. Madey, J.K. Sass and E.M. Stuve, *Surf. Sci.*, *183*, 334 (1987).
9. J.E. Müller and J. Harris, *Phys. Rev. Lett.*, *53*, 2493 (1984).
10. M.W. Ribarsky, W.D. Luedtke and U. Landman, *Phys. Rev.*, *B32*, 1430 (1985).
11. C.W. Bauschlicher Jr., *J. Chem. Phys.*, *83*, 3129 (1985).
12. E. Spohr, *J. Phys. Chem.*, *93*, 6171 (1989).
13. S. Holloway and K.H. Bennemann, *Surf. Sci.*, *101*, 327 (1980).
14. P. Bopp, G. Jancsó and K. Heinzinger, *Chem. Phys. Lett.*, *98*, 129 (1983).
15. K. Foster, K. Raghavan and M. Berkowitz, *Chem. Phys. Lett.*, *162*, 32 (1989).
16. K. Raghavan, K. Foster, K. Motakabbir and M. Berkowitz, *J. Chem. Phys.*, *94*, 2110 (1991)
17. E. Spohr, *Chem. Phys.*, *141*, 87 (1990).
18. E. Spohr and K. Heinzinger, *Ber. Bunsenges. Phys. Chem.*, *92*, 1358 (1988).
19. G. Nagy and K. Heinzinger, *J. Electroanal.*, *296*, 549 (1990).
20. G. Nagy and K. Heinzinger, to be published
21. J. Seitz-Beywl, M. Poxleitner, M.M. Probst and K. Heinzinger, *Int. J. Quantum Chem.*, in press
22. J. Seitz-Beywl, M. Poxleitner and K. Heinzinger, *Z. Naturforsch.*, in press
23. K. Heinzinger, in: *Computer Modelling of Fluids, Polymers, and Solids* (C.R.A. Catlow et al., eds.), Kluwer Academic Publishers, Dordrecht 1990, 357-394.
24. J.E. Black and P. Bopp, *Surf. Sci.*, *140*, 275 (1984).
25. F. Booth, *J. Chem. Phys.*, *19*, 391 (1951).
26. D. Henderson, L. Blum and M. Lozada-Cassou, *J. Electroanal. Chem.*, *150*, 291 (1983).
27. F.H. Stillinger and A. Rahman, *J. Chem. Phys.*, *68*, 666 (1978).
28. G. Jancsó, P. Bopp and K. Heinzinger, *Chem. Phys.*, *85*, 377 (1984).
29. M.G. Sceats and S.A. Rice, *J. Chem. Phys.*, *72*, 3236 (1980).
30. H. Ibach and S. Lehwald, *Surf. Sci.*, *91*, 187 (1980).
31. K. Heinzinger and E. Spohr, *Electrochim. Acta*, *34*, 1849 (1989).
32. E. Spohr, G. Pálinkás, K. Heinzinger, P. Bopp and M.M. Probst, *J. Phys. Chem.*, *92*, 6754 (1988).